



HAL
open science

Carbon monoxide-induced metabolic switch in adipocytes improves insulin resistance in obese mice

Laura Braud, Maria Pini, Lucie Muchova, Sylvie Manin, Hiroaki Kitagishi, Daigo Sawaki, Gabor Czibik, Julien Ternacle, Geneviève Derumeaux, Roberta Foresti, et al.

► To cite this version:

Laura Braud, Maria Pini, Lucie Muchova, Sylvie Manin, Hiroaki Kitagishi, et al.. Carbon monoxide-induced metabolic switch in adipocytes improves insulin resistance in obese mice. *JCI Insight*, 2018, 3 (22), pp.e123485. 10.1172/jci.insight.123485 . inserm-03217223

HAL Id: inserm-03217223

<https://inserm.hal.science/inserm-03217223v1>

Submitted on 4 May 2021

HAL is a multi-disciplinary open access archive for the deposit and dissemination of scientific research documents, whether they are published or not. The documents may come from teaching and research institutions in France or abroad, or from public or private research centers.

L'archive ouverte pluridisciplinaire **HAL**, est destinée au dépôt et à la diffusion de documents scientifiques de niveau recherche, publiés ou non, émanant des établissements d'enseignement et de recherche français ou étrangers, des laboratoires publics ou privés.

1 **Carbon monoxide-induced metabolic switch in adipocytes**
2 **improves insulin resistance in obese mice**

3

4 Laura Braud^{1,2}, Maria Pini^{2,3}, Lucie Muchova⁴, Sylvie Manin^{1,2}, Hiroaki Kitagishi⁵,
5 Daigo Sawaki^{2,3}, Gabor Czibik^{2,3}, Julien Ternacle^{2,3}, Geneviève Derumeaux^{2,3},
6 Roberta Foresti^{1,2*}, Roberto Motterlini^{1,2*}

7

8

9 ¹Inserm U955, Team 12, Créteil 94000, France

10 ²Faculty of Medicine, University Paris-Est, Créteil 94000, France

11 ³Inserm U955, Team 8, Créteil 94000, France

12 ⁴Institute of Medical Biochemistry and Laboratory Diagnostics, 1st Faculty of
13 Medicine, Charles University, Prague, Czech Republic

14 ⁵Department of Molecular Chemistry and Biochemistry, Faculty of Science and
15 Engineering, Doshisha University, Kyotanabe, Kyoto, 610-0321, Japan

16

17 *Corresponding authors: Roberto Motterlini and Roberta Foresti, Inserm U955, Team
18 12, Faculty of Medicine, University Paris-Est, 24 rue du Général Sarrail, 94000
19 Créteil. Phone: +33-149813637. Email address: roberto.motterlini@inserm.fr;
20 roberta.foresti@inserm.fr.

21

22

23

24

25 **Abstract**

26 Obesity is characterized by accumulation of adipose tissue and is one the most
27 important risk factors in the development of insulin resistance. Carbon monoxide-
28 releasing molecules (CO-RMs) have been reported to improve the metabolic profile
29 of obese mice but the underlying mechanism remains poorly defined. Here, we show
30 that oral administration of CORM-401 in high fat diet (HFD) obese mice resulted in a
31 significant reduction in body weight gain accompanied by a marked improvement in
32 glucose homeostasis. We further unmasked a novel action by which CO
33 accumulates in visceral adipose tissue, uncouples mitochondrial respiration in
34 adipocytes ultimately leading to a concomitant switch towards glycolysis. This was
35 accompanied by enhanced systemic and adipose tissue insulin sensitivity as
36 indicated by a lower blood glucose and increased Akt phosphorylation. Our findings
37 indicate that the transient uncoupling activity of CO elicited by repetitive
38 administration of CORM-401 is associated with lower weight gain and increased
39 insulin sensitivity during HFD. Thus, prototypic compounds that release CO could be
40 investigated for developing promising insulin-sensitizing agents.

41

42

43

44

45

46 **Introduction**

47

48 Obesity is one the most important risk factors leading to metabolic dysfunction
49 and type 2 diabetes (1). Excessive accumulation of visceral fat is accompanied by
50 chronic low grade inflammation contributing to the development of insulin resistance,
51 hyperglycemia and adipose tissue dysfunction (2, 3). Whether malfunction of
52 mitochondria, which play a crucial role in cellular bioenergetics, is implicated in
53 adipose tissue dysfunction is still debated (4). Indeed, defective mitochondrial activity
54 can lead to impaired fatty acid oxidation and glycolysis, thereby causing disruption of
55 lipid and glucose metabolism (4). It has also been reported that mitochondrial
56 oxidative stress in adipocytes diminishes insulin-stimulated GLUT4 translocation and
57 glucose uptake resulting in insulin resistance (5). In contrast, an increased glucose
58 tolerance and insulin sensitivity was observed in mice with genetically altered
59 mitochondrial oxidative phosphorylation (6) and an enhanced mitochondrial capacity
60 was described in human subjects with insulin resistance (7). Nevertheless,
61 pharmacological interventions that target mitochondria for the treatment of diabetes
62 have attracted a strong interest over the last decade (8, 9). For example,
63 mitochondrial uncoupling agents such as 2,4-dinitrophenol or niclosamide
64 ethanolamine have demonstrated promising effects on diabetic symptoms in mice by
65 both promoting substrate oxidation and reducing oxidative stress in mitochondria
66 (10, 11).

67 Emerging evidence indicates that carbon monoxide (CO) modulates metabolism
68 in different cell types (12–15). CO is a ubiquitous gaseous molecule produced in
69 mammalian cells and tissues through the breakdown of heme catalyzed by heme
70 oxygenase (HO) enzymes (16). Initially considered as a toxic product, CO is now
71 recognized as a key signaling molecule with vasoactive and cardioprotective effects
72 as well as anti-thrombotic, anti-apoptotic and anti-inflammatory properties (17, 18). In
73 relation to cellular metabolism, we have shown that small amounts of CO increase
74 O₂ consumption in cells via a mild uncoupling activity in mitochondria that is
75 accompanied by changes in the production of reactive oxygen species (12). The use
76 of CO-releasing molecules (CO-RMs), a class of compounds that release controlled
77 quantities of CO into cells and tissues, has helped to unravel this novel mechanism
78 of action and identify the potential therapeutic effects of this gas (12, 17, 19, 20).

79 Accordingly, the water soluble CORM-A1 has been shown to improve dietary-
80 induced obesity, hyperglycemia and insulin resistance in mice (21, 22). However, the
81 mechanisms underlying this beneficial outcome of CO in obesity have been poorly
82 investigated.

83 In the current study, we examined the effect of CORM-401 on whole body insulin
84 sensitivity and glucose tolerance in C57BL6 mice subjected to an obesogenic high
85 fat diet (HFD). We report that oral administration of CORM-401 reduces the gain in
86 body weight and improves insulin resistance in HFD obese mice. CO delivered by
87 CORM-401 to adipose tissue and cells uncouples mitochondrial respiration leading
88 to an increase in glycolysis to maintain ATP levels. This metabolic switch was
89 associated with higher phosphorylation of the insulin signaling effector Akt and was
90 accompanied by an amelioration of systemic and adipocytes insulin sensitivity. Our
91 data demonstrate that the effect of CO on cellular bioenergetics in adipose tissue
92 serves to counteract insulin resistance in obese mice.

93
94
95
96
97

98 Results

99

100 Oral administration of CORM-401 reduces body weight gain and improves 101 insulin resistance in HFD-induced obesity in mice

102 We have shown recently that CORM-401, a manganese-based compound that
103 releases 3 equivalents of CO/mole (Structure shown in Supplemental Table 1),
104 exerts a stronger vasodilatory effect and angiogenic activity than CORM-A1, a boron
105 compound that liberates only 1 CO/mole (20). Thus, it appears that CORM-401
106 exhibits enhanced pharmacological activities due to liberation of higher amounts of
107 CO. Since CORM-401 has never been tested *in vivo*, we first determined the levels
108 of blood COHb in mice receiving CORM-401 at two different doses after oral gavage.
109 Figure 1A and Supplemental Figure 1A show that COHb significantly increased to
110 2.5% and 4.5% 30 min after administration of CORM-401 at 15 and 30 mg/kg,
111 respectively, and gradually decreased to control levels over a period of 48 h. These
112 data confirm that CO is released by CORM-401 and delivered into the circulation in a
113 dose-dependent fashion. Based on this kinetic, we decided to assess the metabolic
114 effects of CORM-401 (15 and 30 mg/kg) administered three times a week to mice
115 fed either a standard diet (SD) or a high fat diet (HFD) for 14 weeks. As shown in
116 Supplemental Figure 1B-E, CORM-401 decreased body weight gain and improved
117 both glucose metabolism and insulin resistance in a dose-dependent manner in HFD
118 mice but the effect was significant only at the dose of 30 mg/kg. Because consistent
119 results were obtained with 30 mg/kg CORM-401, we decided to continue our
120 investigation using this dose in two distinct protocols whereby CORM-401 was given
121 in concomitance with the HFD (prevention group, HFD+CORM-P) or 6 weeks after
122 the beginning of HFD (treatment group, HFD+CORM-T). Body weight gain was
123 significantly increased by the HFD and was reduced by CORM-401 both in the
124 prevention and the treatment group (Figure 1B and C) as reflected by decreased
125 plasma leptin (Figure 1M). Changes in body weight were not due to differences in
126 food intake between the groups (Table 1). In addition, mice fed with SD and
127 SD+CORM-401 displayed similar body weight, suggesting that the compound was
128 well tolerated and the reduced weight gain in HFD-fed mice was not due to a toxic
129 effect of the drug (Supplemental Figure 2A and B). In addition, we did not observe
130 any change in cardiac function parameters by CORM-401 compared to untreated

131 obese mice (Supplemental Table 2). Interestingly, CORM-401 did not affect glucose
132 metabolism in SD mice (Supplemental Figure 2C-F) but improved whole-body
133 glucose tolerance and insulin sensitivity in HFD mice, as shown by a significant
134 decrease in glycemia (Figure 2D and E). In line with this, CORM-401 decreased
135 fasting plasma glycemia and insulin, improving the calculated HOMA-IR in HFD mice
136 (Figure 1 J-L), while plasma cholesterol and triglyceride levels remained unchanged
137 (Figure 1H and I). These results indicate that CORM-401 counteracts body weight
138 gain, impaired glucose tolerance and insulin resistance induced by HFD in mice.

139

140 **CORM-401 remodels adipose tissue in obese mice**

141 We next investigated the effect of CORM-401 on adipose tissue metabolic and
142 inflammatory profiles. Even though eWAT weight was not affected by CORM-401
143 (Figure 2A and B), the size of adipocytes was significantly reduced by 25% in the
144 HFD+CORM-P group (Figure 2A and C). Interestingly, conditioned media of eWAT
145 collected from both mice groups administered with CORM-401 displayed lower non-
146 esterified free fatty acid (NEFA) content compared to the HFD group (Figure 2D).
147 Furthermore, the mRNA expression of the key metabolic genes *PParg*, *Adiponectin*
148 *Fabp4*, *Hsl*, *Glut4*, *Irs1*, *Hk2* and *Vegf* was decreased by the HFD (Figure 2E) and
149 restored to basal levels by CORM-401 in the HFD+CORM-P but not in HFD+CORM-
150 T group. In contrast, mRNA expression of *PPara*, *Pgc1a* and *Cpt1* was decreased by
151 HFD but remained unchanged after CORM-401 treatment (data not shown).
152 Significant remodeling in other fat pads, particularly in brown adipose tissue (BAT),
153 was evident in the reduction of weight and lipid content in both groups administered
154 with CORM-401 (Supplemental Figure 3A-E). Similarly to eWAT, mRNA expression
155 of the metabolic genes *PParg*, *Vegf*, *Adiponectin*, *Pgc1a* and *Ucp1* were decreased
156 in BAT of HFD-obese mice and fully or partially restored in the HFD+CORM-P group
157 (Supplemental Figure 3G). Conversely, gene expression of metabolic markers in
158 subcutaneous adipose tissue (SubWAT) was not affected by CORM-401
159 (Supplemental Figure 3F). Despite the fact that HFD did not induce a high-grade
160 inflammation in our model, CORM-401 still modulated local inflammation in obese
161 mice. First, the increased macrophage infiltration induced by HFD was virtually
162 abolished by CORM-401 administration (Figure 2F-G), although the induction of *Ccl2*
163 was unchanged by the compound (Figure 2H). Secondly, CORM-401 decreased

164 *Hmox-1* expression induced by HFD (Figure 2I) and the levels of IL-6, IL-1 β and IL-
165 10 in eWAT conditioned media (Figure 2J). These data demonstrate that the positive
166 effects of CORM-401 on weight gain and metabolism in obese mice correlate with an
167 amelioration of adipose tissue structure, function and inflammation.

168 CORM-401 had no effect on the liver, another crucial organ for the maintenance
169 of glucose homeostasis. In fact, CORM-401 did not modify the increase in liver
170 weight (1.5-fold) and lipid content caused by HFD (Supplemental Figure 4A-C) and
171 only marginally affected the deregulation of the metabolic genes *PParg*, *Hk2*, *Irs1*,
172 *Hsl*, *Fabp4* induced by HFD (Supplemental Figure 4D). We note that the plasmatic
173 indexes of liver injury were not impacted by HFD (Table 2), suggesting non-
174 advanced hepatic steatosis without major injuries.

175

176 **CO delivered by CORM-401 increases systemic and adipocytes insulin-** 177 **sensitivity**

178 To elucidate whether the improved insulin resistance promoted by CORM-401 is
179 linked to an effect of CO on adipocytes, we assessed insulin sensitivity in eWAT and
180 3T3-L1 adipocytes. We first confirmed that CO content in eWAT increased
181 significantly 2 and 6 h after oral gavage with CORM-401 compared to eWAT from
182 mice treated with PBS (CON) or inactive CORM-401 (iCORM) (Figure 3A). We then
183 determined glucose levels in mice treated with PBS, iCORM or CORM-401 1 h prior
184 to intraperitoneal injection of insulin (Figure 3B) and showed that only CORM-401
185 enhanced systemic insulin sensitivity (Figure 3C and D). In addition, phosphorylation
186 of protein kinase B (Akt) induced by insulin was increased in eWAT from CORM-
187 401-treated mice compared to control (Figure 3E and F). This response was
188 recapitulated in eWAT of obese mice following oral gavage with CORM-401
189 (Supplemental Figure 5). As observed in eWAT, CO content in 3T3-L1 adipocytes
190 exposed to 50 μ M CORM-401 was significantly higher compared to cells treated with
191 PBS or iCORM (Figure 3G). Likewise, only CORM-401-treated adipocytes exhibited
192 increased Akt phosphorylation in basal conditions and after stimulation with insulin
193 (20 nM) for 10 min (Figure 3H, 3I and J). These data demonstrate that CO liberated
194 from CORM-401 accumulates in adipose tissue and regulates Akt signaling to
195 improve insulin sensitivity.

196

197 **CO uncouples mitochondrial respiration and increases glycolytic rate in**
198 **adipocytes**

199 We next investigated the effects of CORM-401 on adipocyte bioenergetics based
200 on the emerging evidence that CO is a metabolic regulator in vascular, inflammatory
201 and cancer cells (12, 23). Using MitoStress assays, we showed that CORM-401-
202 treated 3T3-L1 adipocytes display a concentration-dependent increase in oxygen
203 consumption rate (OCR) even in the presence of the ATP synthase inhibitor
204 oligomycin (Figure 4A and Supplemental Figure 4), resulting in decreased ATP-
205 linked respiration (or coupled respiration) and higher proton leak (or uncoupled
206 respiration) compared to untreated cells (Figure 4B). This effect was followed by
207 reduced respiration in response to the uncoupling agent FCCP and augmented non-
208 mitochondrial respiration after addition of rotenone/antimycin A. These results
209 indicate an uncoupling activity of CORM-401 in adipocytes, as previously observed
210 in other cell types (12). Interestingly, in the absence of inhibitors of the electron
211 transport chain, CORM-401 induced a transient increase in OCR lasting for 2 to 3 h
212 depending on the dose used. This effect was concomitant with a rise in glycolysis as
213 assessed by the extracellular acidification rate (ECAR) (Figure 4C and D).
214 Accordingly, intracellular lactate was increased by CORM-401 (Figure 4E). A
215 glycolysis stress test confirmed that CORM-401, but not iCORM, enhanced ECAR in
216 adipocytes following sequential addition of glucose, oligomycin and 2-DG (Figure 4F
217 and G). Increased glycolysis was not an artifact due to acidification of the medium by
218 CORM-401 since blocking this pathway with 2-DG completely prevented the effects
219 of CORM-401.

220 Notably, intracellular ATP levels were higher in CORM-401-treated adipocytes
221 compared to iCORM, suggesting that glycolysis is engaged as a compensatory
222 mechanism for maintenance of energy (Figure 4H). ATP content was diminished by
223 2-DG in iCORM and CORM-401-treated cells; however, this decrease was more
224 pronounced in adipocytes exposed to CORM-401, likely a result of the uncoupling
225 effect of CO and the inhibition of respiration caused by CORM-401 at the end of the
226 experiment (Figure 4H). We wanted to verify if this metabolic switch induced by
227 CORM-401 occurs in vivo by assessing OCR and ECAR in eWAT collected from
228 mice treated with iCORM or CORM-401 (Figure I). Although no significant
229 differences were observed in basal OCR between the two groups, the response to

230 FCCP was lower after treatment with CORM-401 (Figure 4J), as shown in cultured
231 adipocytes. Most importantly, ECAR was also higher in eWAT punches from CORM-
232 401-treated mice (Figure 4K) and lactate levels in conditioned medium from eWAT
233 collected from mice receiving CORM-401 was increased (Figure 4L), confirming
234 stimulation of glycolysis by CO in vivo.

235

236 **ATP counteracts CO induced-metabolic switch in adipocytes and reverses CO-**
237 **induced increase in insulin sensitivity**

238 Our data indicate that CO induces a metabolic switch, favoring glycolysis, in
239 adipocytes both in vitro and in vivo. If CO decreases mitochondrial ATP production
240 because of transient uncoupling and/or partial inhibition of respiration leading to
241 increased glycolysis to maintain ATP levels, we postulated that ATP *per se* could
242 serve as the molecular trigger of this metabolic switch. To investigate this
243 hypothesis, we artificially delivered ATP packaged in liposomes to adipocytes and
244 examined the effects of CO on bioenergetics. ATP levels significantly increased in
245 adipocytes after exposure to encapsulated-ATP (Figure 5A). Importantly, exogenous
246 ATP supplementation counteracted the rise in ECAR as well as lactate elicited by
247 CORM-401 without affecting the increase in OCR (Figure 5B-D). Furthermore, ATP
248 delivery to adipocytes reversed the increase in insulin-dependent Akt
249 phosphorylation induced by CO (Figure 5E-F). Thus, the suppression of ECAR and
250 Akt phosphorylation by ATP suggests that the increase in glycolysis by CO is a
251 consequence of the uncoupling action of CO and is directly implicated in the
252 improved insulin sensitivity observed in adipocytes.

253

254 **Discussion**

255

256 We report in this study that treatment with the CO-releasing agent CORM-401
257 decreases gain in body weight and markedly ameliorates glucose tolerance and
258 insulin resistance in HFD-induced obese mice. We show that this effect is associated
259 with prevention of adipose tissue alterations as indicated by restoration in metabolic
260 gene expression, suppression of macrophage infiltration and reduction in key
261 inflammatory markers (IL-6, IL-1 β and HO-1) characteristic of obesity. From a
262 mechanistic point of view, we further show that CORM-401: 1) increases insulin
263 sensitivity in adipose tissue by activation of Akt phosphorylation and 2) triggers a
264 metabolic switch that is dependent on mitochondrial uncoupling by CO and is
265 accompanied by an increase in glycolysis and lactate production. These results
266 reveal an important role of CO in regulating bioenergetic metabolism in adipose
267 tissue thus counteracting the deleterious consequences of obesity.

268 We observed that administration of CORM-401 for the whole duration of HFD
269 (CORM-P) was more effective in reducing body weight gain than treatment with
270 CORM-401 starting 6 weeks after the beginning of the HFD regime (CORM-T). This
271 effect is most likely due to a longer period of exposure to CO since we noticed that a
272 significant decrease in body weight becomes apparent in both groups 6 weeks after
273 the first administration of CORM-401. Despite these differences, both groups
274 exhibited the same improvement in glucose tolerance and insulin resistance,
275 suggesting that the effect of CORM-401 on body weight is not the only factor
276 explaining a beneficial role of CO on obesity-induced metabolic dysfunction. Indeed,
277 a lower glycemia and increased insulin sensitivity were also found after one single
278 administration of CORM-401 in lean mice, corroborating a direct pharmacological
279 action of CO on glucose metabolism. When we focused on visceral adipose tissue
280 (eWAT), which undergoes significant structural and functional changes during
281 obesity, we also observed some interesting differences. Although CORM-401 did not
282 affect the increased weight of eWAT in HFD-fed mice, a significant reduction in the
283 size of adipocytes and a restoration of metabolic gene expression were evident in
284 the CORM-P group. These effects correlate with the more pronounced decrease in
285 weight gain in this group. However, both CORM-P and CORM-T groups displayed a
286 similar reduction in the secretion of non-esterified fatty acid, infiltration of

287 macrophages and production of the pro-inflammatory cytokine IL-6 in eWAT,
288 supporting the idea that the pharmacological action mediated by CO on these
289 markers is also independent of the decrease in body weight gain. In particular,
290 inhibition of macrophage infiltration and the marked suppression of IL-6, a cytokine
291 strongly implicated in development of metabolic dysfunction during obesity (24, 25),
292 indicate another potential mechanism by which CORM-401 exerts its beneficial effect
293 on adipose tissue and insulin resistance. We also observed that treatment with
294 CORM-401 diminishes HO-1 gene induction caused by HFD in adipose tissue. This
295 is in line with previous studies showing that HO-1 is increased during HFD in mice
296 (21) and humans (26). HO-1 up-regulation in adipose tissue may be part of the
297 adaptive response mounted by the organism to counteract the inflammatory and
298 metabolic stress elicited by HFD. In fact, systemic induction of HO-1 by cobalt
299 protoporphyrin or genetic over-expression of HO-1 reduces adiposity and improves
300 insulin sensitivity in mice (27–30). However, the role of HO-1 in specific organs
301 involved in metabolic regulation is still controversial since it has also been reported
302 that macrophage and hepatic HO-1 deletion protect against insulin resistance and
303 inflammation (26, 31). Notably, in our study we found that CORM-401 does not have
304 any major effect on the liver. Thus, despite the fact that the liver is a crucial organ for
305 the maintenance of glucose, the findings of this study strongly suggest that the
306 beneficial effect of CO on glucose metabolism is mainly driven by its interaction with
307 adipose tissue.

308 Our results confirm previous findings showing that CORM-A1, another CO-
309 releasing agent, significantly diminishes body weight gain and insulin resistance
310 when given intraperitoneally to HFD-fed mice for 30 weeks (17). A difference in our
311 study is that CORM-401 was administered orally to mice. In addition, we advance
312 the current knowledge on the pharmacological properties of CO-RMs by reporting
313 that a transient increase in COHb levels is associated with accumulation of CO
314 within the adipose tissue. Thus, we demonstrate that CO reaches the adipose tissue
315 and modulates its function in vivo. This finding is further supported by the complete
316 lack of effects by inactive CORM-401, which is depleted of CO. Importantly, we
317 identified that CO directly impacts insulin sensitivity since phosphorylation of Akt, a
318 major pathway implicated in insulin signaling, is significantly enhanced in adipocytes
319 and adipose tissue after CORM-401 treatment. Despite the fact that increased Akt

320 phosphorylation by CO has been reported in other cell types and tissues (32–34),
321 the specific activation of this signal transduction pathway in adipose tissue likely
322 explains the effect of CO on glucose metabolism independently from the reduction in
323 weight gain.

324 The additional mechanism that most likely accounts for an improved glucose
325 tolerance is the switch of adipose tissue metabolism towards glycolysis mediated by
326 CO. This effect was confirmed by increased lactate production in adipocytes and in
327 the secretome of adipose tissue after exposure to CORM-401, suggesting
328 augmented glucose utilization. This metabolic switch occurred in concomitance with
329 a rise in oxygen consumption and a decrease in ATP-linked respiration by CORM-
330 401, which we attribute to an uncoupling activity by CO that we have demonstrated
331 previously in isolated mitochondria as well as in endothelial and microglia cells (12,
332 15, 35–37). Thus, a potential defective ATP production in response to CO-mediated
333 uncoupling would trigger glycolysis as a compensatory mechanism to preserve
334 energy levels leading to improved systemic glucose profile. Indeed, ATP levels were
335 maintained after CORM-401 treatment in adipocytes and were significantly
336 decreased only in the presence of the glycolysis inhibitor 2-deoxyglucose. In
337 addition, direct delivery of ATP into adipocytes prevented the metabolic switch
338 (glycolysis and lactate production) and the increase in insulin sensitivity (Akt
339 phosphorylation) without altering the uncoupling effect caused by CO. That is, when
340 ATP is artificially raised in adipocytes, cells sense adequate energy levels and do not
341 engage glycolysis, even though a diminished mitochondrial ATP production by the
342 uncoupling activity of CO is still occurring. The increase in glycolysis exerted by CO
343 in adipocytes is reminiscent of the action of metformin, an antidiabetic drug well-
344 known to improve insulin resistance in chronic obese patients (38) and capable of
345 inhibiting mitochondrial ATP production (39). Notably, it has been reported that
346 genetic alteration of mitochondrial oxidative phosphorylation improves insulin-
347 sensitivity in mice (6) while enhanced mitochondrial capacity in muscle is associated
348 with higher risk of diabetes in humans (7). It is still debated whether mild increases
349 or decreases in respiratory chain function are beneficial against insulin resistance.
350 Our findings argue in favor of reducing respiratory chain function as a promising
351 approach in the treatment of insulin resistance.

352 Uncoupling agents are renowned to promote weight loss because of their ability to
353 dissipate energy as heat at the expense of ATP production by mitochondria (9, 40).
354 Therefore, we propose that the transient uncoupling activity of CO elicited by
355 repetitive administration of CORM-401 is a prominent mechanism responsible for the
356 lower weight gain during the HFD regime. Because this uncoupling effect is
357 concomitant to enhanced glycolysis, these two actions of CO appear to be essential
358 in the restoration of metabolic homeostasis in obesity (Figure 6).

359 In summary, this study provides the first evidence that an orally active CO-
360 releasing agent is effective in counteracting glucose intolerance and weight gain in
361 HFD obese mice. The ability of CO to interact with mitochondria and improve
362 adipose tissue function seems to be central to this effect. Thus, our findings support
363 the idea that CORM-401 could be investigated as a prototypic compound for the
364 development of promising insulin-sensitizing agents.

365

366 **Materials and methods**

367

368 *Chemicals and Reagents.* CORM-401 ($\text{Mn}(\text{CO})_4\{\text{S}_2\text{CNMe}(\text{CH}_2\text{CO}_2\text{H})\}$) (see
369 chemical structure in Supplemental Figure 1) was synthesized as previously
370 described (41). Stock solutions (5-10 mM) were prepared by solubilizing CORM-401
371 in Dulbecco Phosphate Buffer Solution (pH= 7.4) and stored at -20 °C until use. As a
372 negative control, CORM-401 was inactivated (iCORM) by incubation with equimolar
373 concentrations of hydrogen peroxide for 24 h in order to remove CO from CORM-
374 401. The absence of CO release from iCORM was verified using a hemoglobin
375 assay (see below). For the animal experiments, standard diet (A04) and high fat diet
376 (Purified Diet 230 HF) were purchased from SAFE Diet (Augy, France). Dulbecco's
377 modified Eagle's medium (DMEM), penicillin/streptomycin, dexamethasone, new
378 born calf serum and fetal bovine serum (FBS) were purchased from Life
379 Technologies. Pyruvate, isobutylmethylxanthine (IBMX), insulin and all other
380 reagents were obtained from Sigma Aldrich unless otherwise specified.

381

382 *Animals and experimental design.* Eight-week-old male C57BL6 mice weighing
383 approximately 25 g were obtained from Janvier (France). Mice were housed under
384 controlled conditions of temperature ($21\pm 1^\circ\text{C}$), hygrometry ($60\pm 10\%$) and lighting (12
385 h per day). Animals were acclimatized in the laboratory for one week before the start
386 of the experiments. Mice were fed either a standard diet (SD) or a high fat diet (HFD)
387 for 14 weeks with or without CORM-401 treatment. In preliminary experiments, we
388 tested CORM-401 at 15 mg/kg and 30 mg/kg given orally three times a week to
389 evaluate its dose-dependent effects in our model. Because the effects were more
390 pronounced with 30 mg/kg CORM-401, we continued our study using this dose and
391 randomly divided mice into five groups (n=10 per group): 1) SD mice; 2) HFD mice;
392 3) SD mice administered with CORM-401 starting at week 6 after the beginning of
393 the diet (SD+CORM); 4) HFD mice administered with CORM-401 starting at week six
394 after the beginning of the diet (treatment group, SD+CORM-T); 5) HFD mice
395 administered with CORM-401 starting at the beginning of the diet (prevention group,
396 SD+CORM-P). Mice were weighed weekly and food consumption was measured at
397 week four and eight. The total amount of food was weighed daily in the afternoon
398 and averaged for each mouse to obtain a daily food consumption measurement per

399 mouse. Mice were sacrificed at the end of 14 weeks after a 6 h fasting and 48 h after
400 the last CORM treatment. Blood was collected for biochemistry analysis and
401 epididymal white adipose tissue (eWAT), inguinal white adipose tissue (iWAT),
402 brown adipose tissue (BAT) and liver were removed and weighed. In an additional
403 set of experiments, 6 h-fasted mice were given PBS, iCORM (30 mg/kg) or CORM-
404 401 (30 mg/kg) by oral gavage. Metabolic assays were performed 1 h after CORM-
405 401 administration for one set of experiment and mice were sacrificed 2 h after
406 CORM-401 administration for seahorse experiment and adipose tissue collection.

407

408 *Fasting blood glucose, glucose and insulin tolerance tests.* After 6 h fasting, whole-
409 body glucose tolerance and insulin sensitivity were assessed in all groups at weeks
410 five/six and 12/13 by intraperitoneal glucose (GTT) and insulin (ITT) tolerance tests,
411 respectively. In addition, GTT and ITT were also evaluated 1 h after oral gavage of
412 CORM-401. First, blood was obtained via tail clip to assess fasting blood glucose
413 (Caresens[®] N, DinnoSanteTM). Then, mice received a glucose (1.5 g/kg) or insulin
414 (0.3 UI/kg) solution by intraperitoneal injection and blood glucose was measured at
415 15, 30, 60, 90 and 120 min after the injection. The HOmeostasis Model Assessment
416 of Insulin Resistance (HOMA-IR) adjusted to rodents was calculated as $([\text{glucose}$
417 $(\text{mg/dl})/18] \times [\text{insulin} (\text{ng/ml})/0.0347])/108.24$ as reported (42) The area under the
418 curve (AUC) for the glucose excursion was calculated using Graphpad Prism.

419

420 *Transthoracic Echocardiography.* Transthoracic echocardiography was performed in
421 conscious mice as previously described (43, 44). Briefly, in hand-gripped mice
422 parasternal images were acquired at the level of papillary muscles using a 13-
423 MHz linear-array transducer with a Vivid 7 ultrasound system (GE Medical System,
424 Chicago, IL). Left ventricular dimensions were serially obtained in M-mode and
425 derived parameters were calculated using standard formulas. Left ventricular mass
426 was determined using the uncorrected cube assumption (43, 44). Peak systolic
427 values of strain rate in the anterior and posterior wall were obtained using
428 Tissue Doppler Imaging. Strain rate analysis with EchoPac Software (GE Medical
429 System) was performed offline by a blinded observer. Peak systolic strain rate on 8
430 consecutive cardiac cycles were averaged to reduce the effect of respiratory
431 variations (43, 44).

432

433 *Preparation of eWAT-conditioned medium (eCM).* Epididymal white adipose tissue
434 (eWAT 0.1 g) was collected and kept at room temperature in a 24-well plate with 1
435 ml of DMEM/well. The tissue was minced into $\sim 1 \text{ mm}^3$ pieces and incubated for 1 h
436 at 37°C and 5% CO₂ prior to transferring it into a new plate with fresh DMEM
437 medium containing 4.5 g glucose, 2 mM glutamine, 1% free fatty acid bovine serum
438 albumin, 1% antibiotic and antimycotic solution. eWAT-conditioned medium (eCM)
439 was collected 24 h after incubation and stored at -80°C until analysis.

440

441 *Plasma and eCM analysis.* An enzyme-linked immunosorbent assay (ELISA) kit was
442 used to measure insulin (ALPCO Diagnostics, Salem, NH). Triglycerides (TG), total
443 cholesterol (CHOL), lactate, alanine transaminase (ALAT), aspartate transaminase
444 (ASAT), lactate dehydrogenase, creatinine as well as conjugated and total bilirubin
445 were measured in plasma samples using a Cobas 8000 analyser (Roche,
446 Indianapolis, USA). Cytokines (IL-1 β , IL-10 and IL-6) and leptin were measured in
447 plasma and eCM samples using Mesoscale Multiplex and Single-plex plates,
448 respectively (Mesoscale Discovery, Gaithersburg, USA).

449

450 *Analysis of mRNA expression.* After an initial extraction step by mixing Extract-All
451 (Eurobio, France) and chloroform to samples, total RNA purification was performed
452 with a column extraction Kit (RNeasy Mini[®], Qiagen, Germany). Double-strand cDNA
453 was synthesized from total RNA with the High-Capacity cDNA Reverse Transcription
454 Kit (Life Technologies, Carlsbad, CA). Quantitative real-time PCR (qPCR) was
455 performed in a StepOnePlus Real-Time PCR System using commercially available
456 TaqMan primer-probe sets (Life Technologies, Carlsbad, CA). Gene expression was
457 assessed by the comparative CT ($\Delta\Delta\text{CT}$) method with β -actin as the reference gene.

458

459 *Western Blot Analysis.* Snap-frozen eWAT samples (200 mg) were lysed in cell lysis
460 buffer (Cell Signaling, Danvers, MA France) supplemented with 1%
461 phenylmethylsulfonyl fluoride (PMSF). Protein samples were resolved on 12% bis-
462 Tris gels followed by transfer to nitrocellulose membrane. Antibodies for Akt and
463 phospho-Akt (Ser473) were from Cell Signaling (references #4991 and #4060
464 respectively) and antibodies for β -actin were from Santa Cruz (reference sc-47778).

465 Bands were visualized by enhanced chemiluminescence and quantified using
466 ImageJ software.

467

468 *Histology and immunohistochemistry.* Fresh tissues were fixed in 10% phosphate-
469 buffered formalin overnight. Paraffin wax sections of 5 μm were processed for
470 haematoxylin-eosin (H&E) and CD68 immunostaining. Images were analyzed using
471 ImageJ software.

472

473 *3T3-L1 cell culture.* 3T3-L1 murine pre-adipocytes (reference 088SP-L1-F) were
474 purchased from the ZenBio company (NC, USA) and cultured in an atmosphere of 5
475 % CO_2 at 37 $^\circ\text{C}$ using DMEM supplemented with 10% newborn calf serum For
476 adipocyte differentiation, cells were stimulated with 3T3-L1 differentiation medium
477 containing IBMX (500 μM), dexamethasone (250 nM) and insulin (175 nM) for 2 days
478 after cells reached confluency. The medium was changed to DMEM containing 10%
479 FBS and insulin (175 nM) after 2 days and adipocytes were then kept into DMEM
480 containing only 10% FBS. Prior to the experiments, adipocytes were subjected to
481 serum deprivation for 16 h with DMEM supplemented with 0.5% FBS.

482

483 *Cellular Bioenergetic Analysis.* Bioenergetic profiles of 3T3-L1 adipocytes were
484 determined using a Seahorse Bioscience XF24 Analyzer (Billerica, MA, USA) that
485 provides real-time measurements of oxygen consumption rate (OCR), indicative of
486 mitochondrial respiration, and extracellular acidification rate (ECAR), an index of
487 glycolysis. An optimal cell density of 20,000 cells/well was determined from
488 preliminary experiments. Bioenergetic measurements were performed in FBS- and
489 bicarbonate-free DMEM (pH 7.4) supplemented with 4.5 g/L glucose, 1% glutamax
490 and 1% pyruvate to match the normal culture conditions of 3T3-L1 cells. In a first set
491 of experiments, the effect of CORM-401 (25-100 μM) on OCR and ECAR was
492 assessed over time. In a second set of experiments, the effect of CORM-401 on
493 mitochondrial function was evaluated by means of a MitoStress test, which allows
494 the measurements of key parameters such as ATP-linked respiration and proton leak
495 after sequential additions of: 1 $\mu\text{g/ml}$ oligomycin (inhibitor of ATP synthesis), 0.7 μM
496 carbonyl cyanide 4-(trifluoromethoxy) phenylhydrazone (FCCP, uncoupling agent)
497 and 1 μM rotenone/antimycin A (inhibitors of complex I and complex III of the

498 respiratory chain, respectively). CORM-401 was added 1 h prior to oligomycin to
499 ensure delivery of CO to cells before assessment of mitochondrial function. In an
500 alternative set of experiments, we investigated the effect of CORM-401 on
501 respiration in the absence of ATP synthesis by adding first oligomycin to cells
502 followed by CORM-401, FCCP and rotenone/antimycin A. In a third set of
503 experiments, the effect of CORM-401 on glycolysis was evaluated by means of a
504 Glycolytic stress test, which allow the measurements of glycolysis and glycolytic
505 reserve capacity after sequential additions of: 10 mM glucose, 1 µg/ml oligomycin
506 and 50 mM of 2-deoxyglucose (inhibitor of glycolysis).The pharmacological action of
507 CORM-401 was compared to that of iCORM-401, which does not release CO.

508

509 *ATP Assay.* Intracellular ATP levels were measured using an ATPLite™
510 Bioluminescence Assay Kit (PerkinElmer, France) according to manufacturer's
511 instructions.

512

513 *Assays for the detection of CO in vivo and in vitro.* The levels of carbonmonoxy
514 hemoglobin (COHb) in blood was determined as previously described by our group
515 (45). Briefly, blood (5 µl) collected from the mice tail vein at different time points after
516 oral administration with CORM-401 was added to a cuvette containing 4.5 ml of
517 deoxygenated tris(hydroxymethyl) aminomethane solution and spectra recorded as
518 reported above. The percentage of COHb was calculated based on the absorbance
519 at 420 and 432 nm with the reported extinction coefficients for mouse blood (46).
520 The detection of CO content in adipose tissue following oral gavage with CORM-401
521 was determined by the method of Vreman et al. (47). For this, adipose tissues were
522 initially placed in ice-cold potassium phosphate buffer (1:4 w/v) and stored at -80
523 C_until analysis. The day of the experiment, tissues were diced and sonicated and
524 forty microliters of this suspension was added to CO-free sealed vials containing 5
525 mL of 30% (w/v) sulfosalicylic acid and incubated for 30 min on ice. CO released into
526 the vial headspace was quantified by gas chromatography. CO accumulated in
527 cultured 3T3-L1 adipocytes after traitement with CORM-401 was measured
528 spectrophotometrically using a specific scavenger of CO (hemoCD1) as previously
529 described (48).

530

531 *Statistics.* Data are expressed as mean values \pm standard error of the mean (SEM).
532 Statistical analysis were performed using the unpaired 2-tailed Student's t test or
533 one-way or two-way analysis of variance (ANOVA) with Fisher multiple comparison
534 test. The result were considered significant if the p-value was <0.05 .

535

536 *Study approval.* All animals received care according to institutional guidelines, and
537 all experiments were approved by the Institutional Ethics committee number 16,
538 Paris, France (licence number 16-090).

539

540

541

542 **Author Contributions**

543 L.B., R.F. and R.M. designed the study, performed experiments, collected and
544 analyzed data and wrote the manuscript. L.B. and M.P. performed metabolic tests.
545 L.M. performed CO measurements in adipose tissue. S.M. performed histological
546 staining. H.K. provided critical materials and advice on the use of hemoCD. L.B.,
547 M.P., D.S. and G.C. collected organs for analysis. J.T. performed the
548 echocardiography. G.D. analyzed the echocardiography and read the manuscript.
549 R.M. is the guarantor of this work and, as such, had full access to all the data in this
550 study and takes responsibility for the integrity of the data and the accuracy of the
551 data analysis.

552

553 **Acknowledgements**

554 This work was supported by a grant from the French National Research Agency
555 (ANR) (ANR-15-RHUS-0003). The authors thank Dr. Jayne-Louise Wilson for her
556 support in performing experiments with the Seahorse Analyzer. The authors also
557 thank Rachid Souktani and Cécile Lecointe for help in the animal facility platform;
558 Xavier Decrouy, Christelle Gandolphe and Wilfried Verbecq-Morlot from the
559 histology platform; and Stéphane Moutereau at Henri Mondor Hospital for blood
560 analysis.

561

562 **Conflict of interest:** The authors have declared that no conflict of interest exists.

563

564 **References**

565

566 1. Stumvoll M, Goldstein BJ, van Haeften TW. Type 2 diabetes: principles of
567 pathogenesis and therapy. *The Lancet* 2005;365(9467):1333–1346.

568 2. Guilherme A, Virbasius JV, Puri V, Czech MP. Adipocyte dysfunctions linking
569 obesity to insulin resistance and type 2 diabetes. *Nat. Rev. Mol. Cell Biol.*
570 2008;9(5):367–377.

571 3. Barazzoni R, Gortan Cappellari G, Ragni M, Nisoli E. Insulin resistance in obesity:
572 an overview of fundamental alterations. *Eat. Weight Disord. EWD* 2018;23(2):149–
573 157.

574 4. Montgomery MK, Turner N. Mitochondrial dysfunction and insulin resistance: an
575 update. *Endocr. Connect.* 2015;4(1):R1–R15.

576 5. Fazakerley DJ et al. Mitochondrial oxidative stress causes insulin resistance
577 without disrupting oxidative phosphorylation. *J. Biol. Chem.* 2018;jbc.RA117.001254.

578 6. Pospisilik JA et al. Targeted deletion of AIF decreases mitochondrial oxidative
579 phosphorylation and protects from obesity and diabetes. *Cell* 2007;131(3):476–491.

580 7. Nair KS et al. Asian Indians have enhanced skeletal muscle mitochondrial
581 capacity to produce ATP in association with severe insulin resistance. *Diabetes*
582 2008;57(5):1166–1175.

583 8. Green K, Brand MD, Murphy MP. Prevention of Mitochondrial Oxidative Damage
584 as a Therapeutic Strategy in Diabetes. *Diabetes* 2004;53(suppl 1):S110–S118.

- 585 9. Harper JA, Dickinson K, Brand MD. Mitochondrial uncoupling as a target for drug
586 development for the treatment of obesity. *Obes. Rev.* 2001;2(4):255–265.
- 587 10. Tao H, Zhang Y, Zeng X, Shulman GI, Jin S. Niclosamide ethanolamine–induced
588 mild mitochondrial uncoupling improves diabetic symptoms in mice. *Nat. Med.*
589 2014;20(11):1263–1269.
- 590 11. Crunkhorn S. Metabolic disease: Mitochondrial uncoupler reverses diabetes
591 [Internet]. *Nat. Rev. Drug Discov.* 2014; doi:10.1038/nrd4491
- 592 12. Wilson JL et al. Carbon monoxide reverses the metabolic adaptation of microglia
593 cells to an inflammatory stimulus. *Free Radic. Biol. Med.* 2017;104:311–323.
- 594 13. Lavitrano M et al. Carbon monoxide improves cardiac energetics and safeguards
595 the heart during reperfusion after cardiopulmonary bypass in pigs. *FASEB J. Off.*
596 *Publ. Fed. Am. Soc. Exp. Biol.* 2004;18(10):1093–1095.
- 597 14. Almeida AS, Sonnewald U, Alves PM, Vieira HLA. Carbon monoxide improves
598 neuronal differentiation and yield by increasing the functioning and number of
599 mitochondria. *J. Neurochem.* 2016;138(3):423–435.
- 600 15. Motterlini R, Foresti R. Biological signaling by carbon monoxide and carbon
601 monoxide-releasing molecules. *Am. J. Physiol. - Cell Physiol.* 2017;312(3):C302–
602 C313.
- 603 16. Motterlini R, Foresti R. Heme Oxygenase-1 As a Target for Drug Discovery.
604 *Antioxid. Redox Signal.* 2013;20(11):1810–1826.
- 605 17. Motterlini R, Otterbein LE. The therapeutic potential of carbon monoxide. *Nat.*
606 *Rev. Drug Discov.* 2010;9(9):728–743.

- 607 18. Foresti R, Braud L, Motterlini R. Signaling and Cellular Functions of Carbon
608 Monoxide (CO). In: *Metallobiology Series - Gasotransmitters*. Cambridge, UK: R.
609 Wang; 2018:161–191
- 610 19. Clark JE et al. Cardioprotective actions by a water-soluble carbon monoxide-
611 releasing molecule. *Circ. Res.* 2003;93(2):e2-8.
- 612 20. Fayad-Kobeissi S et al. Vascular and angiogenic activities of CORM-401, an
613 oxidant-sensitive CO-releasing molecule. *Biochem. Pharmacol.* 2016;102:64–77.
- 614 21. Hosick PA et al. Chronic carbon monoxide treatment attenuates development of
615 obesity and remodels adipocytes in mice fed a high-fat diet. *Int. J. Obes.*
616 2014;38(1):132–139.
- 617 22. Hosick PA, AlAmodi AA, Hankins MW, Stec DE. Chronic treatment with a carbon
618 monoxide releasing molecule reverses dietary induced obesity in mice. *Adipocyte*
619 2015;5(1):1–10.
- 620 23. Wegiel B et al. Carbon monoxide expedites metabolic exhaustion to inhibit tumor
621 growth. *Cancer Res.* 2013;73(23):7009–7021.
- 622 24. Cai D et al. Local and systemic insulin resistance resulting from hepatic
623 activation of IKK-beta and NF-kappaB. *Nat. Med.* 2005;11(2):183–190.
- 624 25. Kim H-J et al. Differential effects of interleukin-6 and -10 on skeletal muscle and
625 liver insulin action in vivo. *Diabetes* 2004;53(4):1060–1067.
- 626 26. Jais A et al. Heme Oxygenase-1 Drives Metaflammation and Insulin Resistance
627 in Mouse and Man. *Cell* 2014;158(1):25–40.

- 628 27. Li M et al. Treatment of obese diabetic mice with a heme oxygenase inducer
629 reduces visceral and subcutaneous adiposity, increases adiponectin levels, and
630 improves insulin sensitivity and glucose tolerance. *Diabetes* 2008;57(6):1526–1535.
- 631 28. Ndisang JF, Lane N, Jadhav A. Upregulation of the heme oxygenase system
632 ameliorates postprandial and fasting hyperglycemia in type 2 diabetes. *Am. J.*
633 *Physiol. Endocrinol. Metab.* 2009;296(5):E1029-1041.
- 634 29. Nicolai A et al. Heme Oxygenase-1 Induction Remodels Adipose Tissue and
635 Improves Insulin Sensitivity in Obesity-Induced Diabetic Rats. *Hypertension*
636 2009;53(3):508–515.
- 637 30. Burgess A et al. Adipocyte Heme Oxygenase-1 Induction Attenuates Metabolic
638 Syndrome in Both Male and Female Obese Mice. *Hypertension* 2010;56(6):1124–
639 1130.
- 640 31. Huang J-Y, Chiang M-T, Yet S-F, Chau L-Y. Myeloid heme oxygenase-1
641 haploinsufficiency reduces high fat diet-induced insulin resistance by affecting
642 adipose macrophage infiltration in mice. *PloS One* 2012;7(6):e38626.
- 643 32. Kim HJ et al. Carbon monoxide protects against hepatic ischemia/reperfusion
644 injury via ROS-dependent Akt signaling and inhibition of glycogen synthase kinase
645 3 β . *Oxid. Med. Cell. Longev.* 2013;2013:306421.
- 646 33. Yang P-M, Huang Y-T, Zhang Y-Q, Hsieh C-W, Wung B-S. Carbon monoxide
647 releasing molecule induces endothelial nitric oxide synthase activation through a
648 calcium and phosphatidylinositol 3-kinase/Akt mechanism. *Vascul. Pharmacol.*
649 2016;87:209–218.

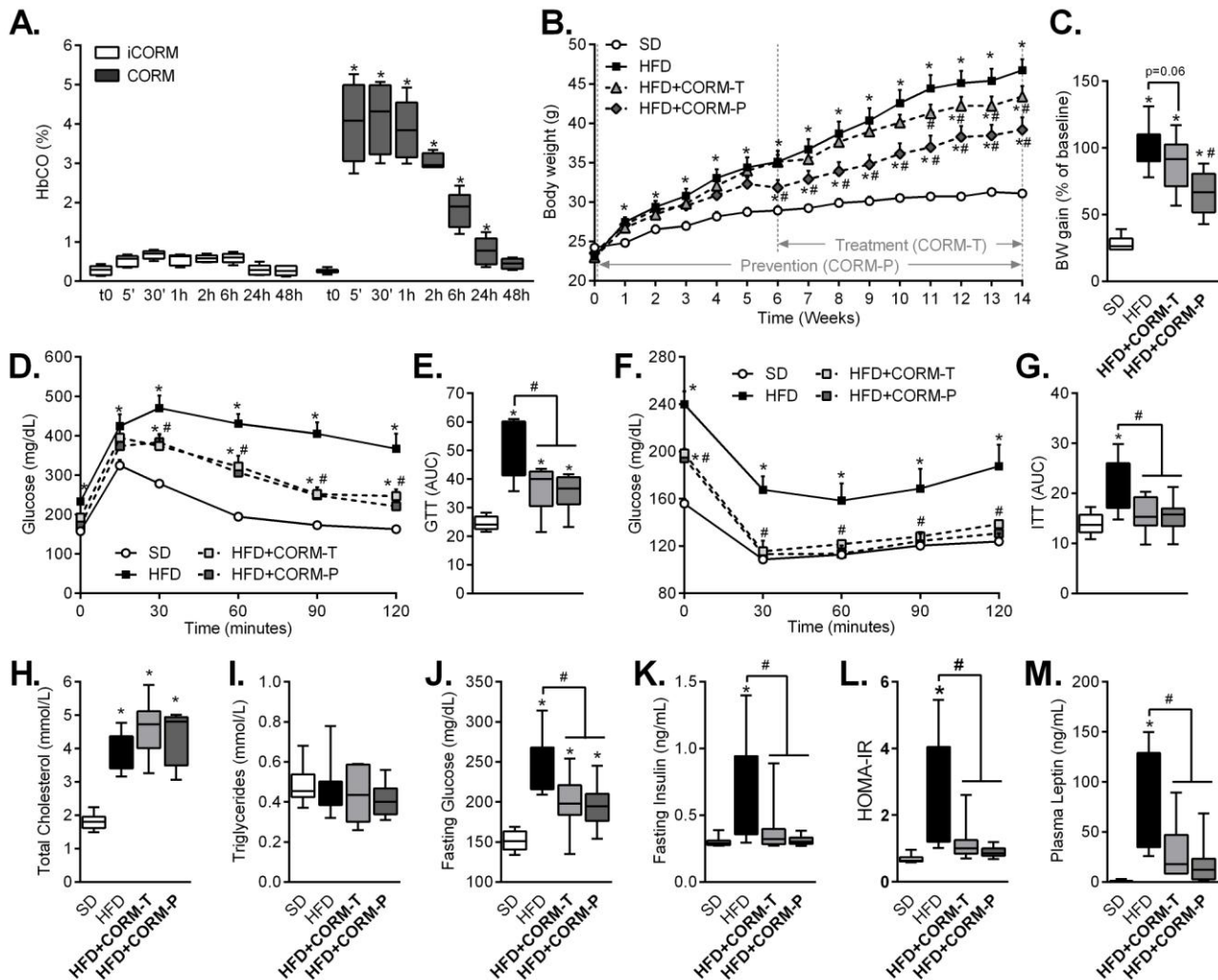
- 650 34. Wegiel B et al. Nitric oxide-dependent bone marrow progenitor mobilization by
651 carbon monoxide enhances endothelial repair after vascular injury. *Circulation*
652 2010;121(4):537–548.
- 653 35. Iacono LL et al. A carbon monoxide-releasing molecule (CORM-3) uncouples
654 mitochondrial respiration and modulates the production of reactive oxygen species.
655 *Free Radic. Biol. Med.* 2011;50(11):1556–1564.
- 656 36. Kaczara P et al. Carbon monoxide released by CORM-401 uncouples
657 mitochondrial respiration and inhibits glycolysis in endothelial cells: A role for
658 mitoBKCa channels. *Biochim. Biophys. Acta* 2015;1847(10):1297–1309.
- 659 37. Sandouka A et al. Carbon monoxide-releasing molecules (CO-RMs) modulate
660 respiration in isolated mitochondria. *Cell. Mol. Biol. Noisy--Gd. Fr.* 2005;51(4):425–
661 432.
- 662 38. González-Barroso MM et al. Fatty acids revert the inhibition of respiration caused
663 by the antidiabetic drug metformin to facilitate their mitochondrial β -oxidation.
664 *Biochim. Biophys. Acta BBA - Bioenerg.* 2012;1817(10):1768–1775.
- 665 39. Zhang Y, Ye J. Mitochondrial inhibitor as a new class of insulin sensitizer. *Acta*
666 *Pharm. Sin. B* 2012;2(4):341–349.
- 667 40. Speakman JR et al. Uncoupled and surviving: individual mice with high
668 metabolism have greater mitochondrial uncoupling and live longer. *Aging Cell*
669 2004;3(3):87–95.
- 670 41. Crook SH et al. $[\text{Mn}(\text{CO})_4\{\text{S}_2\text{CNMe}(\text{CH}_2\text{CO}_2\text{H})\}]$, a new water-soluble CO-
671 releasing molecule. *Dalton Trans. Camb. Engl.* 2003 2011;40(16):4230–4235.

- 672 42. Lee S et al. Comparison between surrogate indexes of insulin sensitivity and
673 resistance and hyperinsulinemic euglycemic clamp estimates in mice. *Am. J.*
674 *Physiol. Endocrinol. Metab.* 2008;294(2):E261-270.
- 675 43. Sawaki D et al. Visceral Adipose Tissue Drives Cardiac Aging Through
676 Modulation of Fibroblast Senescence by Osteopontin Production. *Circulation*
677 [published online ahead of print: March 2, 2018];
678 doi:10.1161/CIRCULATIONAHA.117.031358
- 679 44. Ternacle J et al. Short-term high-fat diet compromises myocardial function: a
680 radial strain rate imaging study. *Eur. Heart J. Cardiovasc. Imaging*
681 2017;18(11):1283–1291.
- 682 45. Nikam A et al. Diverse Nrf2 Activators Coordinated to Cobalt Carbonyls Induce
683 Heme Oxygenase-1 and Release Carbon Monoxide in Vitro and in Vivo. *J. Med.*
684 *Chem.* 2016;59(2):756–762.
- 685 46. Rodkey FL, Hill TA, Pitts LL, Robertson RF. Spectrophotometric measurement of
686 carboxyhemoglobin and methemoglobin in blood. *Clin. Chem.* 1979;25(8):1388–
687 1393.
- 688 47. Vreman HJ, Wong RJ, Kadotani T, Stevenson DK. Determination of carbon
689 monoxide (CO) in rodent tissue: effect of heme administration and environmental CO
690 exposure. *Anal. Biochem.* 2005;341(2):280–289.
- 691 48. Minegishi S et al. Detection and Removal of Endogenous Carbon Monoxide by
692 Selective and Cell-Permeable Hemoprotein Model Complexes. *J. Am. Chem. Soc.*
693 2017;139(16):5984–5991.

694

695

696 **Figure**



697

698 **Figure 1. CORM-401 reduces body weight gain and improves insulin resistance**

699 **in HFD-induced obesity.** Mice received a standard diet (SD) or high fat diet (HFD)

700 for 14 weeks. CORM-401 (30 mg/kg) was given by oral gavage starting either at the

701 beginning (HFD+CORM-T) or after 6 weeks (HFD+CORM-P) HFD. Carbonmonoxy

702 hemoglobin (COHb) was measured after oral gavage with CORM-401 (A). Body

703 weight (BW) was measured every week (B) and BW gain was calculated as

704 percentage of the basal weight (C). A glucose tolerance test (GTT) was performed at

705 week 13 (D) and data represented as the area under the curve (GTT AUC) (E). An

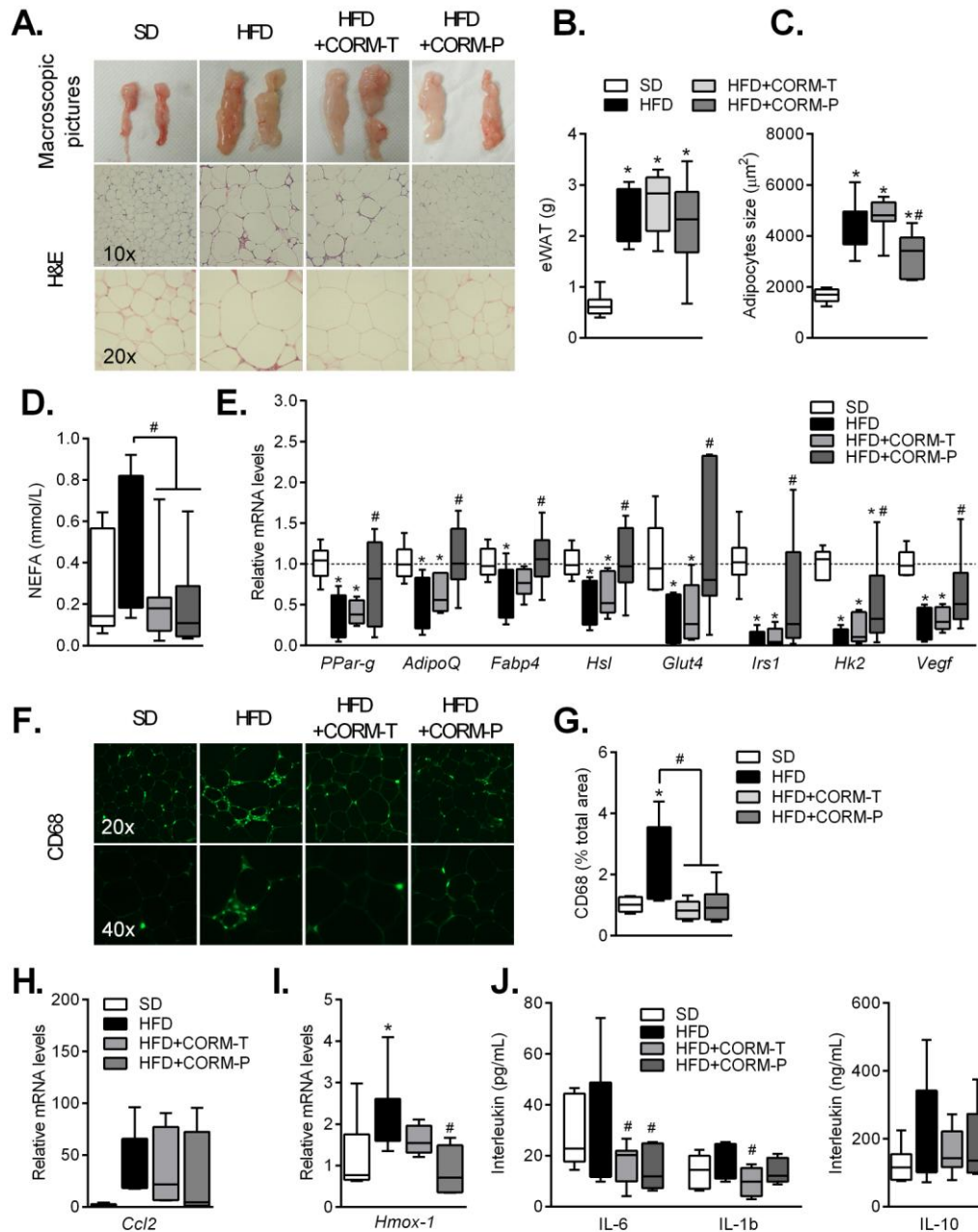
706 insulin tolerance test (ITT) was performed at week 14 (F) and data represented as

707 the area under the curve (ITT AUC) (G). Fasting total cholesterol (H), fasting

708 triglycerides (I), fasting glucose (J), fasting insulin (K), calculated HOMA-IR (L) and

709 fasting leptin (M) were measured after 14 weeks in all groups examined. Values

710 represent the mean \pm SEM. A=4-6 mice per group; B-M=8-10 mice per group.
711 * $p < 0.05$ vs. control group (SD) and # $p < 0.05$ vs. HFD group, values not designated
712 with symbols are not statistically different, student's t test or one-way or two-way
713 ANOVA with Fisher multiple comparison test.
714



715

716 **Figure 2. CORM-401 improves visceral adipose tissue function in HFD-induced**

717 **obesity.** Mice on standard (SD) or high fat diet (HFD) were sacrificed after 14

718 weeks. CORM-401 (30 mg/kg) was given by oral gavage starting either at the

719 beginning (HFD+CORM-T) or after 6 weeks (HFD+CORM-P) HFD. Pictures and

720 representative sections of epididymal white adipose tissue (eWAT) stained with

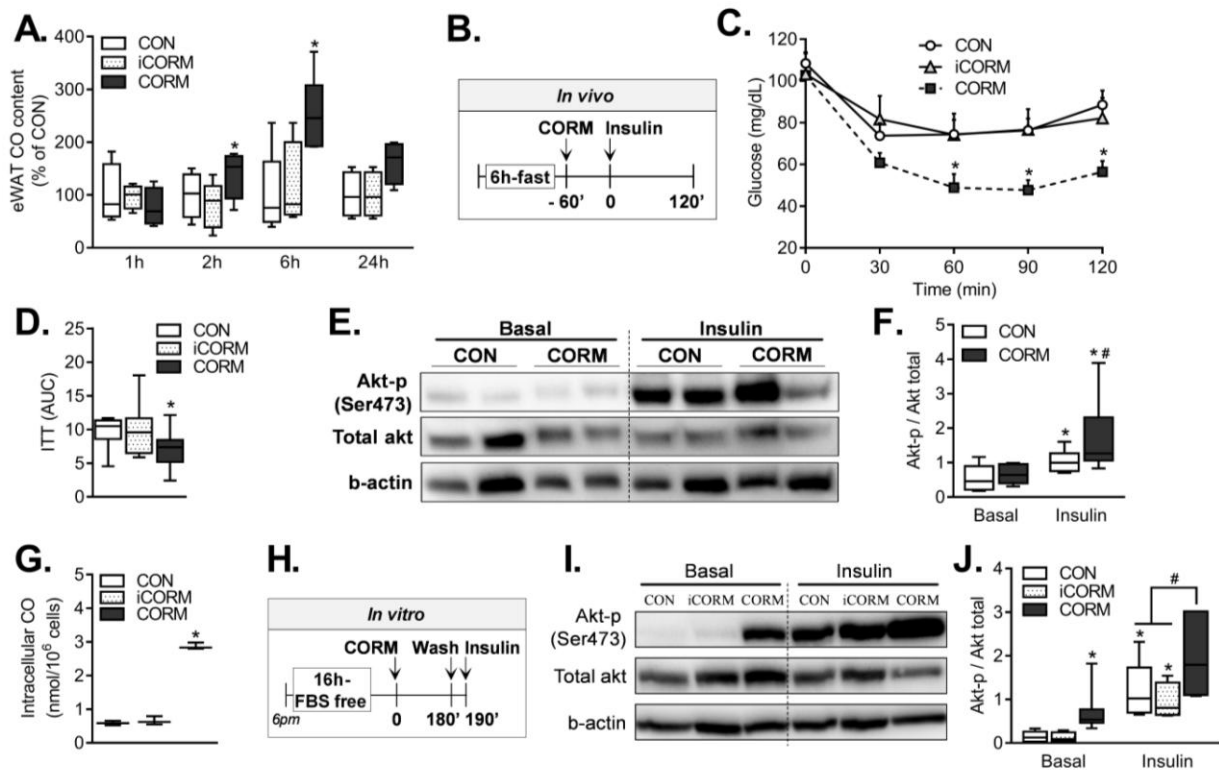
721 hematoxylin-eosin (A). eWAT was also evaluated for weight (B), adipocytes size (C),

722 free fatty acids (FFA) levels from conditioned media (D), mRNA expression of genes

723 involved in metabolism (E), CD68 expression (F, G), mRNA expression of *CCl2* (H)

724 and *Hmox-1* (I) as well as interleukins content from conditioned media (J). mRNA

725 expression was determined by real-time PCR and normalized to β -actin. Values
726 represent the mean \pm SEM, n=6-8 mice/group. *p<0.05 vs. control group (SD) and
727 #p<0.05 vs. HFD group, values not designated with symbols are not statistically
728 different, one-way ANOVA with Fisher multiple comparison test.
729



730

731

732

733

734

735

736

737

738

739

740

741

742

743

744

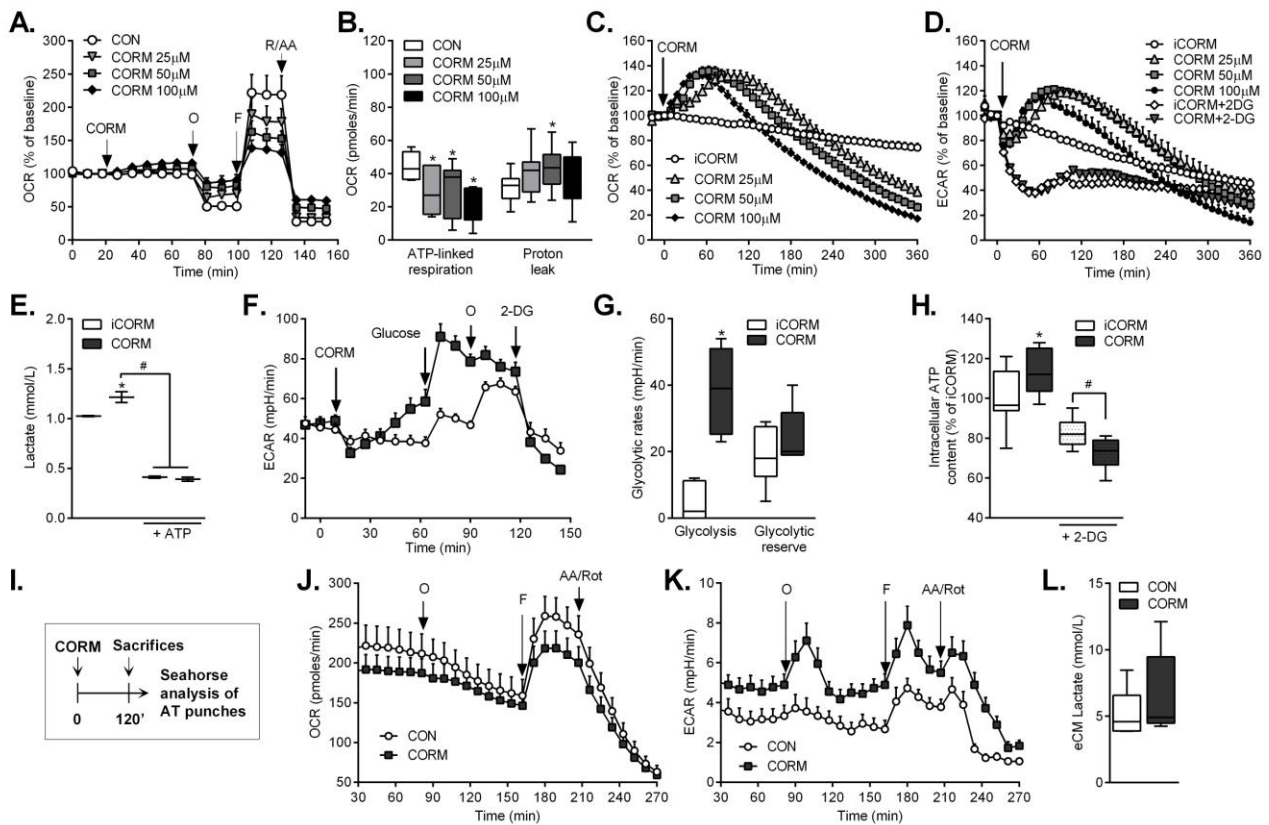
745

746

747

748

Figure 3. CO delivered by CORM-401 increases systemic and adipocytes insulin sensitivity both in vivo and in vitro. CO content was measured in epididimal white adipose tissue (eWAT) after oral gavage with PBS (CON), inactive CORM that does not release CO (iCORM, 30 mg/kg) or CORM-401 (30 mg/kg) (A). An ITT was performed in fasted mice 1 h after oral gavage with PBS (CON), iCORM (30 mg/kg) or CORM-401 (30 mg/kg) (B), while blood glucose levels were measured at the times indicated (C) and represented by area under the curve (ITT AUC) (D). eWAT was evaluated for protein expression of total Akt and phosphorylated Akt assessed by western blot (E, F). Intracellular CO level in 3T3-L1 adipocytes after CORM-401 exposure at 50 μ M for 3 h (G). Proteins were extracted from quiescent 3T3-L1 adipocytes after 3 h exposure to PBS (CON), iCORM (50 μ M) or CORM-401 (50 μ M) (see protocol in H). Expression of total Akt and phosphorylated Akt was assessed by western blot (F, G). Results are expressed as mean \pm SEM. A=4-6 mice per group; C-D=10 mice per group; E-F=8 mice per group; G=3 in triplicates, J=4 independent experiments. * p <0.05 vs. control group (CON) and # p <0.05 vs. insulin, values not designated with symbols are not statistically different, one-way ANOVA with Fisher multiple comparison test.

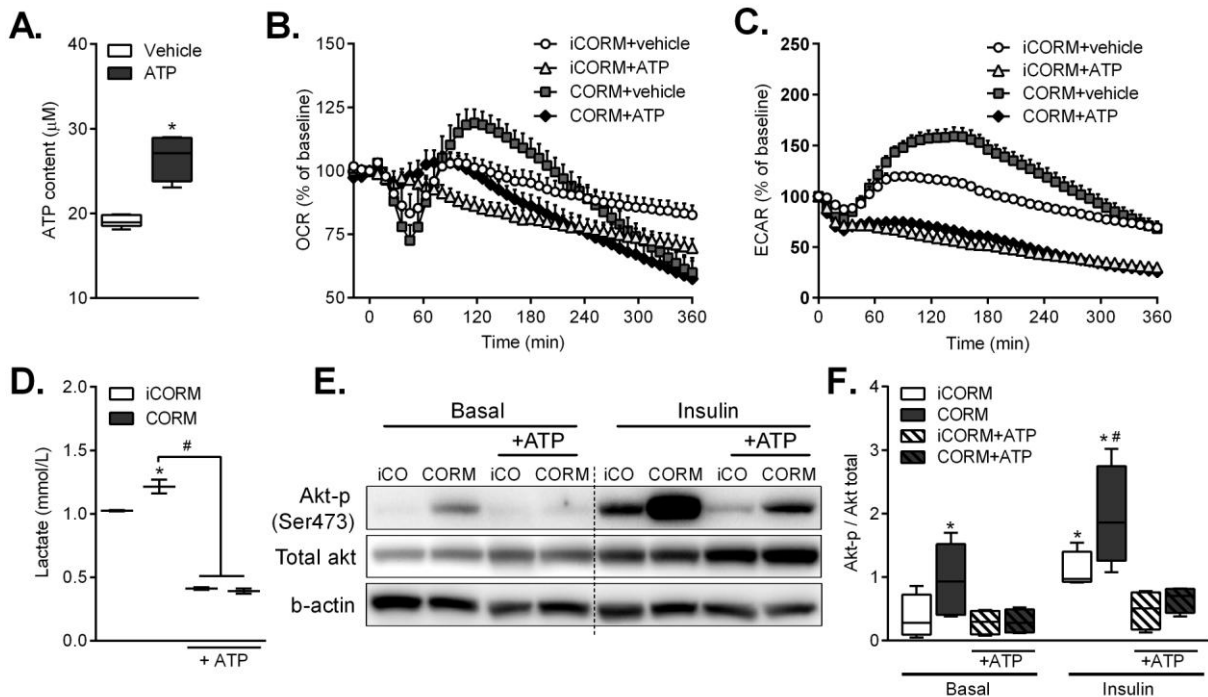


749

750 **Figure 4. CO induces a metabolic switch in adipocytes in vitro and in vivo.**

751 Oxygen consumption rate (OCR) and extracellular acidification rate (ECAR) were
 752 measured in 3T3-L1 cells after addition of PBS (CON) or CORM-401 (25, 50, 100
 753 μM). A MitoStress assay was performed on 3T3-L1 adipocytes after first addition of
 754 PBS or CORM-401 followed by sequential addition of oligomycin, FCCP and
 755 rotenone/antimycin A (A). ATP-linked respiration rate was calculated by subtracting
 756 OCR values after oligomycin addition from basal OCR values and proton leak was
 757 calculated by subtracting OCR values after R/AA addition from OCR values after
 758 oligomycin addition (B). OCR (C) and ECAR (D) were measured for 6 h after addition
 759 of CORM-401. Lactate (E) and intracellular ATP (H) were measured 3 h after
 760 exposure to iCORM or CORM-401 with or without 2-deoxyglucose (2-DG). A
 761 glycolytic assay was performed after addition of iCORM or CORM-401 (50 μM)
 762 followed by sequential addition of glucose, oligomycin and 2-DG (F). Glycolysis rate
 763 was calculated by subtracting ECAR values after glucose addition from basal ECAR
 764 values and glycolytic reserve was calculated by subtracting ECAR values after
 765 oligomycin addition from basal ECAR values (G). Experiments using the Seahorse
 766 Analyzer were performed on punches of eWAT collected from mice 2 h after oral

767 gavage with iCORM or CORM-401 (30 mg/kg) (see protocol in I) and OCR (J) and
768 ECAR (K) were measured. Lactate was measured in eWAT conditioned media (L).
769 Results are expressed as mean \pm SEM. A-D & F-H=4 independent experiments; C=3
770 independent experiments; J-L=6 mice per group. * $p < 0.05$ vs. control group (CON)
771 and # $p < 0.05$ vs. 2-DG, values not designated with symbols are not statistically
772 different, student's *t* test or one-way ANOVA with Fisher multiple comparison test.
773



774

775 **Figure 5. ATP counteracts CO induced-metabolic switch in adipocytes and**

776 **reverses CO-induced increase in insulin sensitivity.** Intracellular ATP (A) was

777 measured after exposure of vehicle (H₂O) or ATP encapsulated in liposome. OCR

778 (B) and ECAR (C) were measured for 6 h after addition of iCORM (50 µM) or CORM-

779 401 (50 µM) with or without vehicle (H₂O) or ATP encapsulated in liposome. Lactate

780 content (D) after exposure of iCORM or CORM-401 with or without ATP. Expression

781 of total Akt and phosphorylated Akt assessed by western blot (E, F). Results are

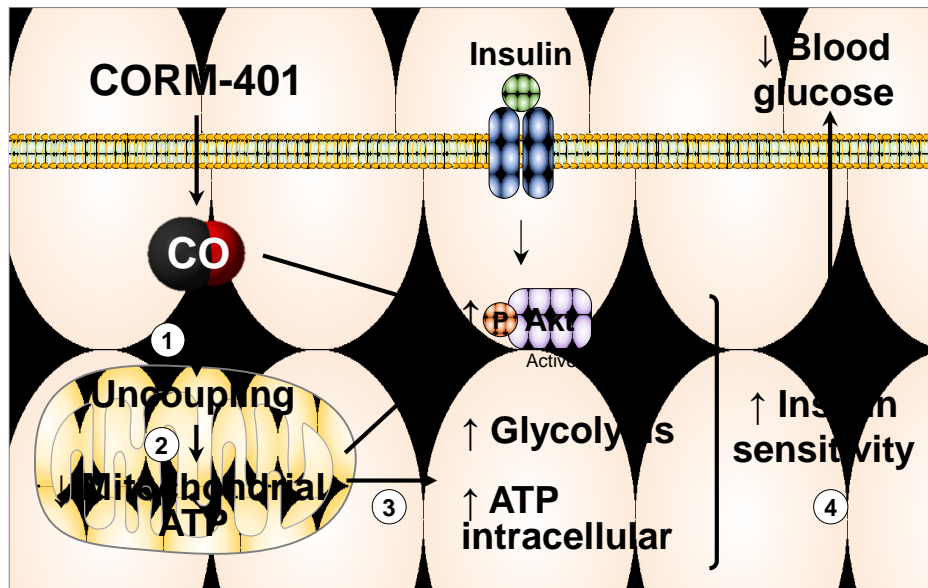
782 expressed as mean ± SEM. n=3-4 independent experiments. *p<0.05 vs. control

783 group (CON) and #p<0.05 vs. insulin, values not designated with symbols are not

784 statistically different, student's *t* test or one-way ANOVA with Fisher multiple

785 comparison test.

786



787

788

789 **Figure 6. Proposed mechanism for the beneficial effects of CO on glucose**
 790 **metabolism in adipose tissue leading to improvement in glucose homeostasis**
 791 **in obese mice.** Obesity is characterized by adipose tissue dysfunction leading to
 792 insulin resistance and fasting hyperglycemia. CO delivered by CORM-401 in adipose
 793 tissue causes an uncoupling of mitochondrial respiration (1) resulting in a transient
 794 decrease in mitochondrial ATP production (2). As counteracting mechanism to this
 795 effect, glycolysis is stimulated in cells leading to maintenance to global intracellular
 796 ATP content (3). This metabolic switch in adipocytes improves local and systemic
 797 insulin sensitivity (4). A transient increase in adipose tissue insulin sensitivity
 798 resolves adipose tissue dysfunction as well as insulin resistance caused by obesity.

799

800

801 **Tables**

802

803 **Table 1. Food intake**

Food intake (g/mouse/day)¹⁻²	SD	HFD	HFD+CORM-T	HFD+CORM-P
<i>4th week</i>	3.8 ± 0.2 ^a	2.8 ± 0.2 ^b	2.8 ± 0.2 ^b	2.6 ± 0.3 ^b
<i>8th week</i>	3.6 ± 0.1 ^a	3.1 ± 0.1 ^b	3.0 ± 0.2 ^b	2.7 ± 0.1 ^b

804 ¹Results are means ± SEM; ²Means with different superscript letters are significantly
805 different among the same period (before treatment or during treatment), $p < 0.05$,
806 one-way ANOVA with Fisher multiple comparison test.

807

808

809

810

811 **Table 2.** Blood analysis

	SD	HFD	HFD+CORM-T	HFD+CORM-P
ASAT/ALAT	3.0 ± 0.5 ^a	2.5 ± 0.9 ^a	3.6 ± 0.9 ^a	2.9 ± 0.7 ^a
Conjugated bilirubin (µmol/L)	0.62 ± 0.2 ^a	0.47 ± 0.07 ^a	0.46 ± 0.06 ^a	0.36 ± 0.03 ^a
Total bilirubin (µmol/L)	6.46 ± 2.1 ^a	4.8 ± 2.1 ^a	7.4 ± 2.2 ^a	4.82 ± 1.9 ^a
Creatinine (mmol/L)	8 ± 0.8 ^a	10.13 ± 1.8 ^a	8.37 ± 1.0 ^a	7.43 ± 1.5 ^a
Lactate deshydrogenase (U/L)	191.2 ± 56.3 ^a	248.1 ± 46.5 ^a	321.3 ± 93.8 ^a	238 ± 66.3 ^a

812 ALAT: Aspartate amino transferase, ASAT: Alanine amino transferase. ¹Results are
 813 means ± SEM; ²Means with different superscript letters are significantly different, $p <$
 814 0.05, one-way ANOVA with Fisher multiple comparison test.

815